

This is the **accepted version** of the article:

Navarro Senent, Cristina; Quintana Romero, Alberto; Isarain-Chávez, Eloy; [et al.]. «Enhancing magneto-ionic effects in magnetic nanostructured films via conformal deposition of nanolayers with oxygen acceptor». ACS Applied Materials and Interfaces, Vol. 12, Issue 12 (March 2020), p. 14484-14494. DOI 10.1021/acsami.9b19363

This version is available at <https://ddd.uab.cat/record/233370>

under the terms of the  **CC BY** COPYRIGHT license

Enhancing magneto-ionic effects in magnetic nanostructured films via conformal deposition of nanolayers with oxygen getter/donor capabilities

Cristina Navarro-Senent,^{,†} Alberto Quintana,^{†,‡} Eloy Isarain-Chávez,[†] Eugen Weschke,[§] Pengmei Yu,^{||} Mariona Coll,^{||} Eva Pellicer,[†] Enric Menéndez,^{†,*} and Jordi Sort^{†,⊥,*}*

[†]Departament de Física, Universitat Autònoma de Barcelona, E-08193 Cerdanyola del Vallès, Spain.

[‡]Department of Physics, Georgetown University, Washington, D.C. 20057, USA

[§]Helmholtz-Zentrum Berlin für Materialien und Energie, Albert-Einstein-Strasse 15, D-12489 Berlin, Germany

^{||}Institut de Ciència de Materials de Barcelona (ICMAB-CSIC) Campus UAB, E-08193 Bellaterra, Catalonia, Spain

[⊥]Institució Catalana de Recerca i Estudis Avançats (ICREA), Pg. Lluís Companys 23, E-08010 Barcelona, Spain

* Corresponding Authors: cristina.navarro.senent@uab.cat, enric.menendez@uab.cat, jordi.sort@uab.cat

ABSTRACT

Effective electric-field manipulation of the magnetic properties of nanostructured metallic alloys exhibiting inter-grain porosity (i.e., channels) conformally coated with insulating oxide nanolayers is demonstrated. Nanostructured Co–Pt films are prepared by electrodeposition (ED) and subsequently coated with either AlO_x or HfO_x by atomic layer deposition (ALD) to promote magneto-ionic effects (i.e., voltage-driven ion migration) during electrolyte-gating. Pronounced variations in coercivity (H_C) and magnetic moment at saturation (m_S) are observed at room temperature after biasing the heterostructures. The application of a negative voltage results in a decrease of H_C and an increase of m_S , whereas the opposite trend is achieved for positive voltages. Although magneto-ionic phenomena are already observed in uncoated Co-Pt films (due to the inherent presence of oxygen), the ALD oxide nanocoatings serve to drastically enhance the magneto-ionic effects due to partially reversible voltage-driven oxygen migration across the interface between AlO_x or HfO_x and the nanostructured Co–Pt film. Co–Pt/ HfO_x heterostructures exhibit the most significant magnetoelectric response at negative voltages, with an increase of m_S up to 76% and a decrease of H_C by 58%. The combination of a nanostructured magnetic alloy and a skin-like insulating oxide nanocoating is shown to be appealing to enhance magneto-ionic effects, potentially enabling electrolyte-gated magneto-ionic technology.

Keywords: magneto-ionic effects, ion migration, voltage control of magnetism, Co-Pt, nanostructured material

INTRODUCTION

Over the last decades, a great deal of effort has been made towards the development of energy-efficient materials and processes in the field of digital communication and information. Spintronics, which makes use of the electronic charge and spin degrees of freedom, has contributed to this progress with novel devices such as spin-transfer torque magnetic random-access memories (STT-MRAM), giant magnetoresistance sensors (GMR) or tunnel magnetoresistance sensors (TMR), among others.^{1,2} So far, the aforementioned devices and technologies have required of electric currents for their operation, which involves an important energy dissipation in the form of heat (Joule effect). To overcome this drawback, a flurry of research has focused, in recent years, on the voltage control of magnetism (*i.e.*, replacing electric currents by electric fields whenever possible, therefore minimizing Joule heating effects and improving energy efficiency in these magnetoelectronic devices).³⁻⁵

Magnetoelectric effects have been accomplished by different strategies, which include: (i) strain-mediated magnetoelectric coupling in piezoelectric-magnetostrictive composite materials,⁶⁻⁸ (ii) single-phase multiferroics materials with intrinsic coupling between ferroelectric and ferromagnetic order parameters⁸⁻¹⁰ and (iii) charge carrier electronic band modulation in certain metallic ferromagnetic materials, typically Fe–Pd, Fe–Pt, Cu–Ni or Co–Pt systems.¹¹⁻¹⁵ Unfortunately, these approaches suffer from some drawbacks: piezoelectric response in piezoelectric/magnetostrictive devices is affected by clamping effects with the substrate and its endurance is in any case limited by fatigue-induced mechanical failure; single-phase multiferroic materials exhibit weak magnetoelectric coupling and only very few of them exhibit multiferroic properties at room temperature¹⁰; electric charge accumulation in metallic materials occurs within the first nanometers from the metal surface due to the short electric-field screening length (the Thomas-Fermi screening length is $\lambda_{TF} \sim 0.5$ nm), limiting magnetoelectric effects to a few nm from the surface, thereby restricting this effect to ultrathin films¹² and nanoporous magnetic alloys.^{11,14}

Alternatively, magneto-ionics is emerging as a novel pathway to tailor magnetism with voltage, which averts the above-mentioned drawbacks. Magneto-ionics relies on the motion of ions (*e.g.* O^{2-} ¹⁶⁻²¹ or Li^{+} ²²⁻²⁴), driven by an electric field, as an effective mechanism for controlling the oxidation-reduction processes of the ferromagnetic material. Interestingly, magnetic properties such as saturation magnetization (M_S),^{19,20,23,25} magnetic anisotropy,^{20,26} coercivity (H_C),^{16,19,25} or Dzyaloshinskii–Moriya interaction (DMI)²⁷ can be successfully manipulated by electrical means taking advantage of ion diffusion. Contrary to the other magnetoelectric mechanisms, magneto-ionic effects are not limited to the electric-field screening length and can be significant even in relatively thick films. Nonetheless, thermal treatments are often required since ion migration is a thermally-activated phenomenon.^{5,17,28}

Within magneto-ionics, most studies have focused so far on metal/metal-oxide flat layers, where the voltage-induced O^{2-} migration is used to tailor magnetism. Commonly, such heterostructures comprise a magnetic material (*e.g.* Fe, Co or Ni) in direct contact to a gate oxide that acts as the oxygen source/sink (*e.g.* GdO_x ,^{16,28} or HfO_2 ^{19,20,27,29}). The applied gate voltage can displace the O^{2-} ions from the metal oxide to the ferromagnetic layer, consequently inducing changes in H_C , M_S , magnetic anisotropy or domain wall velocity, among others.^{16,19,20,27} Interestingly, some of these works use liquid electrolytes (*e.g.* ionic liquids) to achieve large electric fields at the surface of the target material. Upon voltage application, an electric double layer (EDL) is formed at the interface between the oxide layer and the electrolyte, generating reasonably high electric fields (due to the very narrow thickness of the EDL, which is around 0.5 nm)³⁰, thus promoting the oxygen migration through the gate oxide/metal layer.^{19,20,29} Similarly, recent studies have reported changes in different magnetic parameters (magnetic anisotropy, M_S , H_C and even magnetic phase transitions) through direct non-aqueous electrolyte gating, *i.e.*, without assistance of gate oxides layers. In such cases, the source of oxygen is the magnetic material itself (either containing oxygen in its bulk structure or as a surface passivation layer).^{25,26,31-34}

In general, all magnetoelectric phenomena are interface-driven, being thin films the most utilized materials in voltage control of magnetism. Nevertheless, in the last decade, tremendous progress has been made in the synthesis of nanoporous materials for widespread applications in chemistry (adsorption and separation of gas molecules, chemoresistive gas sensors, energy conversion and storage, heterogeneous catalysis, etc.).^{35–37} This has triggered the idea of using nanoporous materials, which exhibit very large surface-to-volume ratios, as potential candidates for maximizing magnetoelectric effects.^{11,14,25,31,38–41} Considering that magneto-ionics is an interfacial effect, where the metal/metal oxide or metal/ionic liquid interface plays a crucial role in the ionic migration, nanoporous morphologies are expected to promote the diffusion of ions; notwithstanding, there are only a few reports on magneto-ionics in nanoporous/mesoporous materials and only a small fraction of them are focused on voltage-induced oxygen migration.^{25,31,38,41}

In a previous study, we demonstrated that the magnetic properties of nanoporous Co–Pt/CoO micro-disks, prepared by electrodeposition (ED), can be easily modulated at room temperature upon voltage application using an anhydrous electrolyte.³¹ The electric charge accumulation at the surface of the ultra-narrow pore walls and the concomitant voltage-driven oxygen migration (magneto-ionic effect) were mainly responsible for the observed effects. However, the amount of available oxygen was limited, since it comprised only the CoO contained in the micro-disks. As a result, only a reduction of H_C and an increase of the Kerr amplitude after applying negative voltage were observed, followed by the recovery of the original values at positive voltages.³¹

In this article, we explore the enhanced voltage-induced oxygen motion in nanostructured Co–Pt/ AlO_x and Co–Pt/ HfO_x heterostructured films gated using an anhydrous electrolyte. First, nanostructured Co–Pt films (with inter-grain porosity and a certain amount of oxygen) are prepared by micelle-assisted ED^{14,31,42,43} from a solution free from pH buffering and complexing agents to allow the formation of cobalt oxides.³¹ Subsequently, atomic layer deposition (ALD) is used to conformally coat with high accuracy the nanoroughened surface and the nanochannels of the Co–Pt

film either with AlO_x or HfO_x nanolayers (two oxides with oxygen vacancy mobility and dissimilar oxygen affinity⁴⁴⁻⁴⁷). In fact, ALD is the most suitable deposition technique to fill the inter-grain nanochannels of the ferromagnetic layer with the aforementioned oxides, thus maximizing the available interface between the ferromagnetic material and the oxide. This strategy is expected to enhance the magneto-ionic effects on the Co–Pt film, where the incorporation of an adjacent oxide nanolayer enables the control of the oxygen content in the ferromagnetic layer. Our work shows that the combination of micelle-assisted ED of a ferromagnetic nanostructured alloy with ALD of suitable oxide nanocoatings is an appealing synthesis pathway to boost magneto-ionic phenomena. The idea is applicable not only to liquid electrolyte gating but also to solid state devices, for example to flexible electronics (*e.g.*, filling porous scaffolds with ionic liquid gels).⁴⁸⁻⁵⁰

RESULTS AND DISCUSSION

The fabrication of the heterostructured films was conducted in two steps. First, nanostructured Co–Pt films (with some degree of inter-grain porosity) were fabricated by micelle-assisted ED. This synthesis approach is employed to prepare mesoporous metals by taking advantage of micelles as a soft template (see **Experimental Section** for details). **Figure 1a,b** shows a top-view scanning electron microscopy (SEM) image of the as-prepared nanostructured Co–Pt film. The film exhibits a homogeneous nanoparticulate morphology composed by nanometer-sized grains with a visible nanostructuring inside each grain which provides a great nano-roughness along the surface (**Figure 1b**). Further structural analysis was performed by scanning transmission electron microscopy (STEM), where a characteristic columnar-like film growth and the presence of inter-grains nanochannels can be appreciated (**Figure 1c**). STEM measurements also show that the overall film thickness is around 150 nm. Energy-dispersive X-ray (EDX) spectroscopy shows that the O, Co, and Pt contents are approximately 38 ± 3 , 48 ± 2 and 14 ± 1 at.%, respectively, with an average composition around $\text{Co}_{77}\text{Pt}_{23}$ considering only the metallic fraction, revealing the growth of a Co-rich alloy.

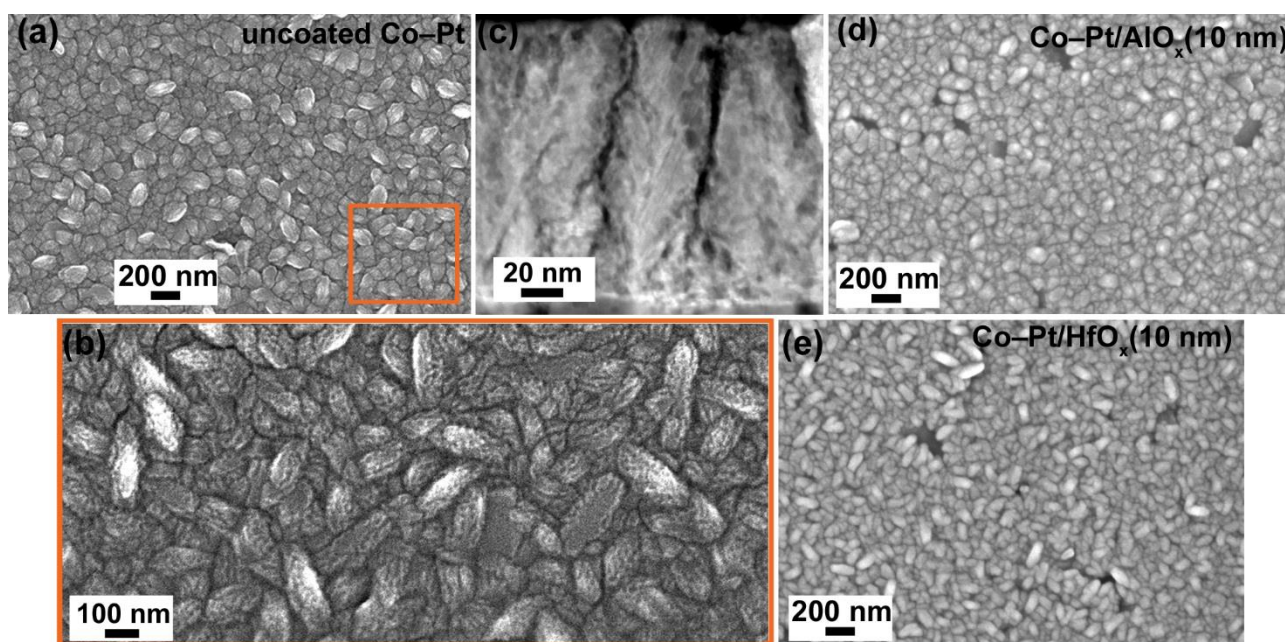


Figure 1. Top-view SEM image of the nanostructured Co–Pt film at (a) low, (b) high magnifications. In panel (b) nanoroughened surface and inter-grain porosity of nanometer size are visible. (c) STEM image of a cross-section of the film. (d,e) Top-view SEM images of (d) Co–Pt/AlO_x and (e) Co–Pt/HfO_x films.

Subsequently, AlO_x and HfO_x nanolayers, with thicknesses of 10 nm, were directly deposited onto the nanostructured Co–Pt films by ALD. Top-view SEM images of the Co–Pt/AlO_x and Co–Pt/HfO_x composite nanostructured films are shown in **Figure 1d,e** respectively. For comparison, the SEM image of the uncoated nanostructured Co–Pt film is also shown. It can be seen that the morphology of the Co–Pt films was preserved after 10 nm AlO_x and HfO_x deposition suggesting that, as expected, the ALD proceeded conformally covering the nanoroughened surface and penetrating into the inter-grain channels (**Figure 1d,e**). Thicker coatings (20 and 80 nm) were also obtained (**Figure S1a,b**). As can be seen in **Figure S1b**, 80 nm-thick coatings cause a sort of flattening of the Co–Pt films morphology probably due to the sealing of the inter-grain channels.⁵¹ The thinnest coatings (10 nm) were selected for magnetoelectric measurements since the insertion of HfO_x and AlO_x adds to the original thickness of the EDL, thus progressively weakening the achievable electric field for a given voltage. To confirm the conformal coating of the nanostructure with the ALD

nanolayer, electron energy loss spectroscopy (EELS) mappings were conducted on a Co–Pt/HfO_x film (**Figure 2**). STEM images of a cross section of a Co–Pt/HfO_x film are shown in **Figure 2**, together with the corresponding Co (red) and Hf (green) EELS mapping in the interfacial area enclosed within the orange box. The EELS mappings reveal the presence of Hf inside the channels of the Co–Pt film, indicating that HfO_x coating has penetrated several tens of nm towards the interior of the Co–Pt film. EELS analyses also show the presence of both Co and Hf at the interfaces between Co–Pt and HfO_x, suggesting that mixed cobalt/hafnium oxides may co-exist within these regions. These results prove that ALD is suitable to conformally coat and fill the inter-grain nanochannels of Co–Pt film, enhancing the interface area between the Co–Pt and the HfO_x nanocoating, thus maximizing magneto-ionic effects.

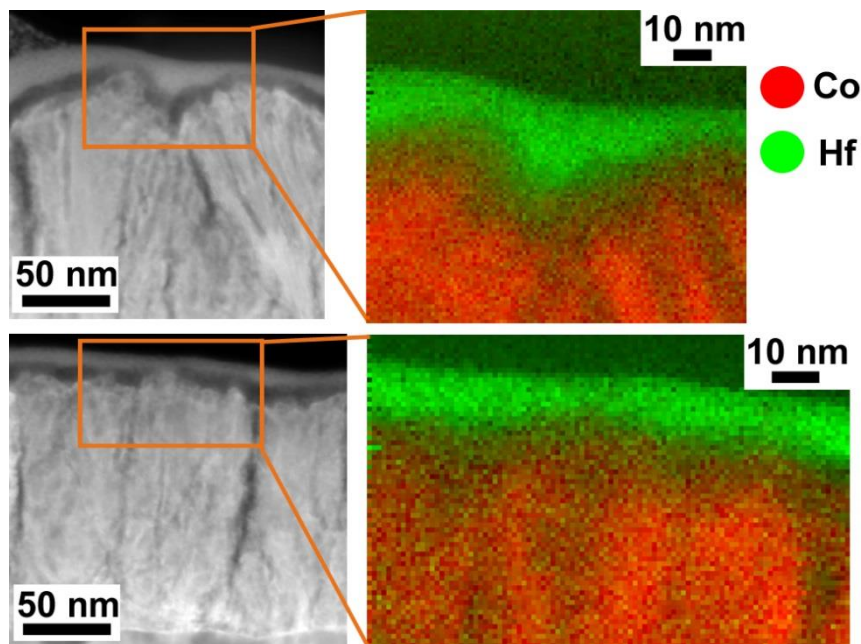


Figure 2. STEM images and corresponding Co and Hf EELS mapping of the area enclosed in the orange box of two regions of a Co–Pt/HfO_x film. Co is in red while Hf is in green.

The crystallographic structure of the uncoated and ALD-coated nanostructured Co–Pt films was characterized by grazing incidence X-ray diffraction (GIXRD). The diffraction pattern of the uncoated film indicates the coexistence of several phases: hexagonal close-packed (hcp) Co, face-centered cubic (fcc) Co, cubic Co₃O₄ and cubic CoO phases (black curve, **Figure 3**). The presence of

these cobalt oxides phases was also detected by EELS mappings, where the co-existence of oxygen and cobalt-rich regions was observed at the inter-grains (**Figure S2**). Note that a slight angular shift in the hcp- and fcc-Co peaks is observed towards small angles compared to the tabulated patterns, indicating an increase in the lattice cell parameter, which is compatible with a dissolution of Pt into the hcp- and fcc-Co lattices. The same crystallographic structure is seen in the patterns of the Co–Pt/ AlO_x and Co–Pt/ HfO_x heterostructured films (red and blue curves in **Figure 3**).^{52–54} No additional peaks attributed to Al_2O_3 or HfO_2 are observed, likely because their amorphous-like nature.⁴³

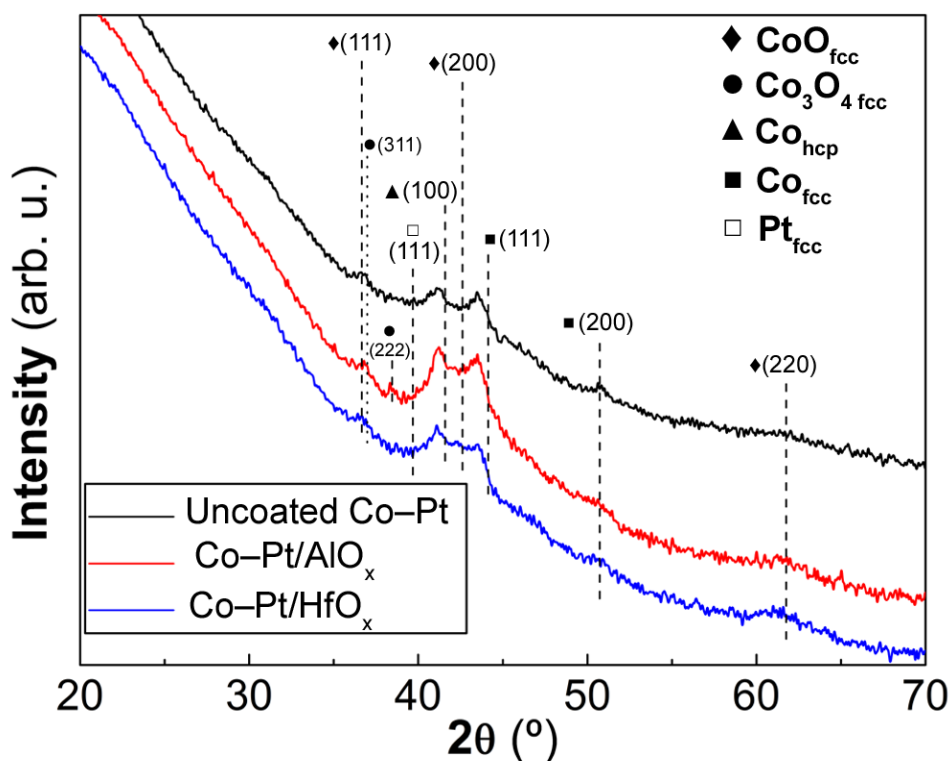


Figure 3. Grazing incidence X-ray diffraction (GIXRD) patterns of the uncoated Co–Pt (black curve) Co–Pt/ AlO_x (10 nm) (red curve) and Co–Pt/ HfO_x (10 nm) (blue curve) films.

Magnetic properties were measured prior to voltage application in a vibrating sample magnetometer (VSM) at room temperature. A decrease of m_s accompanied by a small increase of H_C was observed after coating the Co–Pt film (See Supporting Information, **Figure S3**). Such changes are ascribed to the partial oxidation of Co–Pt during the ALD process, likely occurring at interfacial level, because the coating process involves high temperature (200 °C) for both AlO_x and HfO_x depositions and,

additionally, ozone gas for the AlO_x growth.⁴³ To investigate the electric-field effect on the magnetic properties, hysteresis loops were measured in-plane (always in the same direction) while the films were subjected to different constant negative and positive voltages in an electrolyte. The voltage was applied by using a home-made electrolytic cell containing the films as working electrode, a Pt wire as counter electrode and anhydrous propylene carbonate (PC) with dissolved Na⁺ and OH⁻ ions, as electrolyte (See **Experimental Section**).^{25,32}

For the magnetoelectric experiments, the hysteresis loops of uncoated Co–Pt, Co–Pt/AlO_x and Co–Pt/HfO_x films were recorded by applying different negative voltages ranging from 0 to –100 V after a waiting time of 90 min at each voltage (**Figure 4a,b and c**, respectively). For the sake of clarity, representative loops at selected voltages are shown (see **Figure S4, Supporting Information**, for additional data). Note that differences in the initial magnetic moment among the three samples is due to their dissimilar lateral size. As can be seen in **Figure 4a,b and c**, the loops at 0 V and –3 V are virtually overlapped (black and red loops), indicating that no significant magnetoelectric effects are induced at small voltages. This suggests the existence of an onset voltage, in agreement with previous results.³¹ Conversely, significant variations were observed for all three samples after overcoming the threshold voltage (–7 V, blue loop, **Figure 4a,b and c**), where *m_s* increases and *H_C* decreases as the applied voltage is made progressively more negative. The origin of this threshold voltage is probably related to the bond-dissociation energy between O and Co. This threshold is the minimum energy required for creating O²⁻ ions and inducing the migration of the ions through the film.

After having applied negative voltages, the voltage was removed, and the system was left for a “relaxation period” of 8 h (brown loops, **Figure 4d, e and f**). Subsequently, hysteresis loops were taken at different positive voltages ranging from 0 to +100 V (again waiting 90 min at each voltage) and selected loops are plotted in **Figure 4d, e and f** (see all measured loops in **Figure S4, Supporting Information**). When positive voltages are applied, *m_s* decreases for the three samples (**Figure 4d,e and f**), and even beyond the initial *m_s* value for the uncoated Co–Pt (initial *m_s* = 5.7·10⁻⁴ emu and

$m_S (+100 \text{ V}) = 2.1 \cdot 10^{-4} \text{ emu}$), and, particularly, for Co–Pt/ AlO_x films (initial $m_S = 16.5 \cdot 10^{-4} \text{ emu}$ and $m_S (+50 \text{ V}) = 3.9 \cdot 10^{-4} \text{ emu}$) (**Figure S4a,b**). This already suggests that AlO_x may act as oxygen donor. In contrast, H_C increases slightly upon applying positive voltages (**Figure 4d,e and f**), but does not completely return to the initial values for Co–Pt and Co–Pt/ HfO_x films (**Figure S4a,c**). On the contrary, H_C increases almost back to its initial value at +50 V for the Co–Pt/ AlO_x films (dark blue loop, **Figure S4b**). Thus, Co–Pt/ HfO_x films did not recover the initial state, showing only slight variations in H_C and m_S values (**Figure 4f** and **Figure S4c**). Conversely, as can be seen in **Figure 4e**, the Co–Pt/ AlO_x film polarized at +50 V shows an open loop since the induced magnetoelectric response could not reach a stationary value in spite of the 90 min waiting time at this voltage prior to the hysteresis loop acquisition. In other words, the magnetic properties of this sample kept changing over time while the loop was recorded (approximately 40 min). It should be noted that the Co–Pt/ AlO_x film detached from the substrate at larger positive voltages (+75 and +100 V). Delamination was not observed in the uncoated Co–Pt and Co–Pt/ HfO_x films, indicating that the Co–Pt/ AlO_x coating is less stable at high positive voltages.

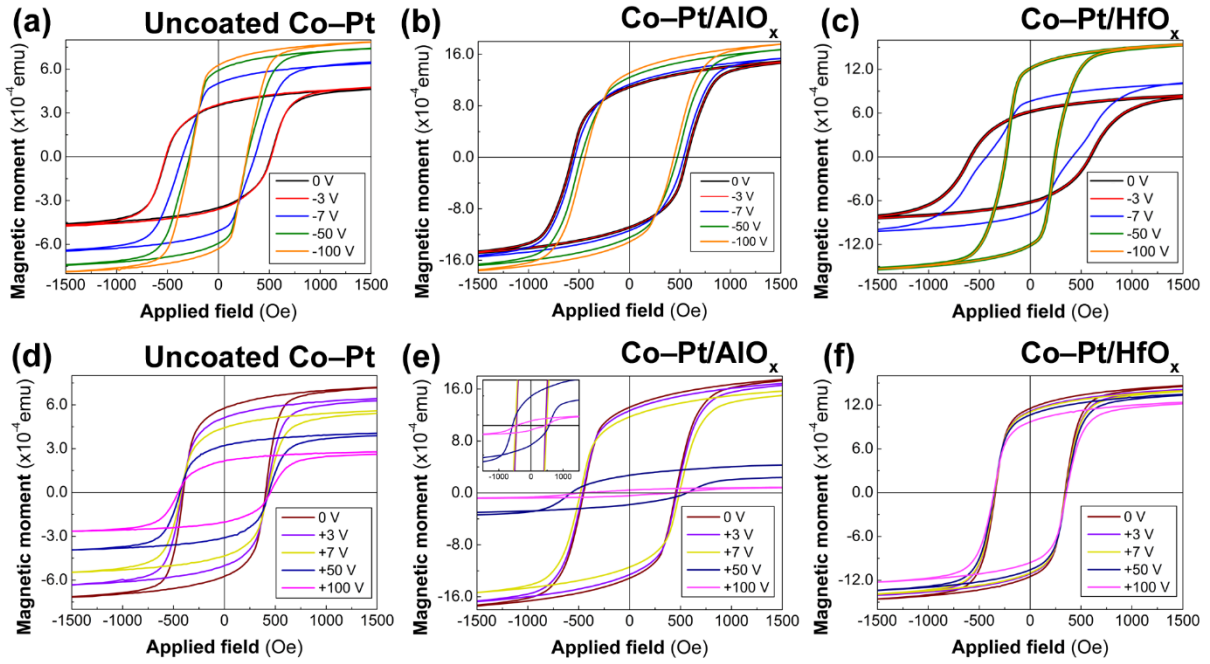


Figure 4. Room temperature in-plane VSM measurements of (a,d) uncoated Co–Pt, (b,e) Co–Pt/ AlO_x and (c,f) Co–Pt/ HfO_x samples after applying 0, –3, –7, –50, –100 V and 0, +3, +7, +50, +100 V for 90 min, respectively.

The results indicate that the relative variations on magnetic properties induced by the applied voltage (*i.e.*, magneto-ionic effects) in each sample differ from one another. For the sake of better understanding, **Figure 5** shows the relative changes in H_C , m_s and remanence to saturation ratio (m_R/m_S) as a function of the applied voltage for the three studied samples. Remarkably, the largest variation of H_C , m_s and m_R/m_S at negative voltages is achieved for Co–Pt/ HfO_x , with a 58% reduction, 76% and 11% increases, respectively (blue curve, **Figure 5a,b and c**). Also remarkable is that, for negative voltages, a plateau is observed for the three magnetic parameters at a value between –20 V and –50 V, suggesting that the voltage effect tends to saturate beyond that applied voltage. In contrast, Co–Pt/ AlO_x exhibits the lowest relative variations of H_C , m_s and m_R/m_S . Conversely, for positive voltages, Co–Pt/ AlO_x shows the largest variation of H_C (25% increase), m_s (81% decrease) and m_R/m_S (10% decrease) (red curve, **Figure 5d,e and f**). Note that these values have been obtained considering the range from 0 V to +50 V (*i.e.*, excluding the +75 V and +100 V points), since the sample Co–Pt/ AlO_x damaged at the upper positive voltages.

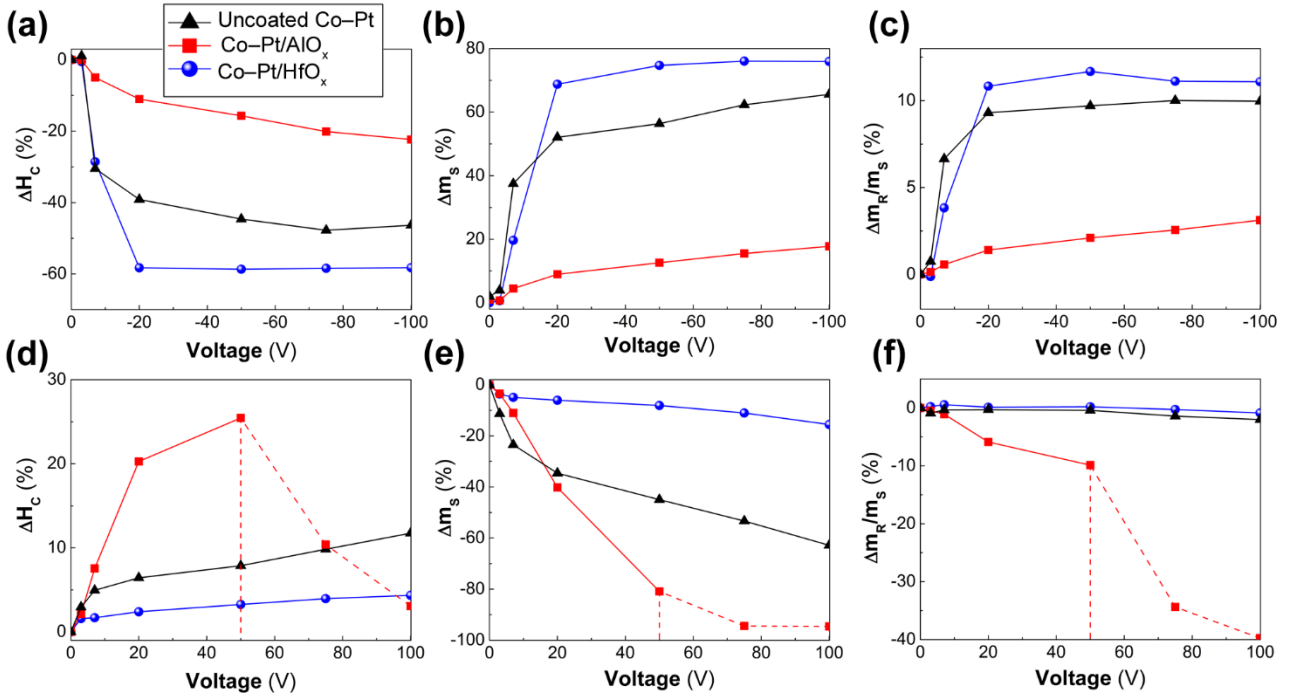


Figure 5. Dependence of the relative variation (%) of (a,d) coercivity (H_C), (b,e) magnetic moment at saturation (m_s) and (c,f) remanence to saturation ratio (m_R/m_s) as a function of the applied negative (a-c) and positive (d-f) voltages. Dashed vertical lines denote film detachment.

In general, the same trends are observed for the three systems, *i.e.*, uncoated Co-Pt, Co-Pt/ AlO_x and Co-Pt/ HfO_x films. The observed modulation in the magnetic behavior of the Co-Pt is attributed to voltage-driven oxygen migration. Indeed, changes are in the same direction as those reported in the literature for the same gating polarity (note that, in our work, the Co-Pt based films act as the gate).^{16,17,19,20,55} Negative voltages cause a decrease of H_C and an increase of m_s . The latter is consistent with a partial reduction of the Co oxides already present in the as-deposited nanostructured Co-Pt layer to metallic Co.³¹ Subsequently, when positive voltages are applied, the re-oxidation of the previously formed metallic Co takes place, resulting in a decrease of m_s . For the uncoated Co-Pt film, such variations originate from voltage-driven O and Co redistributions, as previously reported.³¹ In contrast, for ALD-coated Co-Pt films, the presence of the HfO_x and AlO_x nanolayers has a strong influence on the O^{2-} migration through the Co-Pt/oxide interface depending on the voltage polarity. Namely, for negative applied voltages, the relative change in H_C , m_s and m_R/m_s is the largest for the

Co–Pt/HfO_x, whereas smaller variations are observed in Co–Pt and Co–Pt/AlO_x (**Figure 5a,b and c**). Conversely, Co–Pt/AlO_x is the one that exhibits more pronounced magnetoelectric effects for positive voltages. In other words, the ALD-coated Co–Pt films exhibit higher relative variations than its uncoated counterpart, but to achieve such enhancement, the voltage sign needs to be selected depending on the type of oxide nanocoating. This indicates that the ALD coatings enhance the O²⁻ migration somehow within the Co–Pt layer. Therefore, the role of these ALD nanocoatings as oxygen acceptor/donor materials is important to understand the enhancement of the magneto-ionic effects. Considering that the origin of the observed changes relies on the reduction of the CoO and Co₃O₄ to Co,³¹ the HfO_x coating seems to facilitate the reduction of cobalt oxides upon negative voltage application (*i.e.*, it plays an oxygen getter role⁴⁶). Conversely, AlO_x coating boosts the oxidation of Co at positive voltage (*i.e.*, oxygen donor role⁴⁵). Thus, the results suggest that HfO_x is prone to accept oxygen from the Co–Pt layer, while AlO_x is instead an oxygen donor. In fact, HfO_x have been extensively used as gate oxide material for electrical control of magnetism, where oxygen migration can occur upon voltage application.^{19,20,29,56} However only a few works have reported magneto-ionic effects using AlO_x,^{57,58} where instead of oxygen, Al³⁺ ions could migrate from AlO_x to the ferromagnetic film.⁵⁸ The magneto-electric changes observed for the three samples are attributed to variations in the Co oxidation state in the Co–Pt film; notwithstanding, a possible contribution from Pt could still take place and should not to be completely ruled out. Recent studies have reported changes on the induced magnetic moment of Pt biased by an electric field,⁵⁹ nonetheless, such variations in our work are expected to be minor compared to the induced changes on the Co.

To shed light on the voltage-driven O migration mechanism through the Co–Pt layer, X-ray absorption spectroscopy (XAS) was performed on the uncoated Co–Pt and Co–Pt/HfO_x films at the Cobalt L_{2,3}-edges (black curves, **Figure 6a,c and 6b,d** respectively). For clarity, the L₂ data have been omitted from **Figure 6**, but it is available in the Supporting Information (**Figure S5**), and also the XAS measurements of the Co–Pt/AlO_x films have been omitted, due to their aforementioned poor

stability when subject to positive voltages. Nevertheless, they can be found in **Figure S6**. X-ray magnetic circular dichroism (XMCD), which refers to the difference in absorption for right-handed (μ^+) and left-handed (μ^-) circularly polarized X-rays, was also performed in order to probe the magnetic moment of Co on the uncoated Co–Pt and Co–Pt/HfO_x films (**Figure S7** and **Figure 7**). It should be noted that the detection depth probed by XAS in total electron yield mode when using soft X-rays is limited to the outermost nanometers from the surface, while VSM probes the whole film volume because it is an integrating technique.

The XAS spectrum prior to voltage application of the uncoated Co–Pt film exhibits a multiplet structure consisting of four peaks (777.4, 778.7, 779.1 and 780 eV) at the L₃ edge and a broad peak (794 eV) at the L₂ edge (black curves, **Figure 6a** and **Figure S5a**). The pattern matches the CoO reference XAS spectrum (green curve, **Figure 6a** and **Figure S5a**), although the three main peaks at 778.7, 779.1 and 780 eV are less pronounced in the uncoated Co–Pt film. This sample shows XMCD signal, thus also indicating the presence of ferromagnetic metallic Co (black curve, **Figure S7**). Overall, the results indicate the presence of CoO and metallic Co in the uncoated Co–Pt films, in agreement with its GIXRD pattern (black curve, **Figure 3**). Nonetheless, the presence of small amounts of Co₃O₄ cannot be fully ruled out from XAS and actually, a contribution from this phase in amorphous form is envisaged in the GIXRD pattern (**Figure 3**). After subjecting the uncoated Co–Pt sample to –100 V (XAS was carried out *ex situ*, 30 min elapsed before starting XAS analysis), the four peaks previously observed (776.4, 778.7, 779.1 and 780.5 eV) become more pronounced at the L₃ edge (red curve, **Figure 6c**), while the main peak at L₂ edge is slightly shifted towards higher photon energies (red curve, **Figure S5c**). This, together with the decrease on the dichroic signal (red curve, **Figure S7**), suggests that the amount of CoO increases whereas that of metallic Co decreases upon negative voltage application in the probed volume. When a positive voltage is applied (+100 V), the XAS exhibits a decrease of the shoulder at 776.4 eV and the two peaks at 778.7 and 779.1 eV, which are characteristic of CoO, at the L₃ edge. Moreover, a new peak at 780.6 eV is observed at

the L_3 edge, while the main peak at L_2 edge becomes sharper (blue curve, **Figure S5c**). These features suggest the presence of traces of Co_3O_4 (see orange curve of the Co_3O_4 XAS reference, **Figure 6a** and **Figure S5a**). The results, together with the absence of dichroism in the XMCD signal (blue curve, **Figure S7**), indicate that the sample consists of a mixture of CoO and Co_3O_4 after application of a strong positive voltage.

The observed changes on the XAS data for the uncoated Co-Pt films after negative voltage application seem contradictory with the obtained macroscopic magnetic measurements (**Figures 4** and **5**), where the value of m_s is found to increase (rather than decrease). The XAS results can be understood on the basis of an O migration towards the surface of the nanostructured alloy from Co_3O_4 - and CoO -rich regions. First, when negative voltage is applied, O^{2-} ions from CoO and Co_3O_4 phases migrate towards the surface driven by the electric field. As a result, inner CoO is partially reduced to Co , eventual Co_3O_4 is reduced to CoO and the outmost metallic Co clusters are partially oxidized to CoO . This scenario is schematically depicted in **Figure 8a,b**. Thereby, the redistribution of O across the film leads to the formation of Co -rich inner regions, which is consistent with the increase in m_s (**Figure 4a** and **Figure 5b**), and CoO -rich regions at the surface, which is consistent with the XAS pattern (red curve, **Figure 6c**). Afterwards, when the voltage polarity is reversed (+100 V), O^{2-} ions from the Co_3O_4 are prone to migrate towards the Co/CoO , oxidizing the metallic Co to CoO (**Figure 8c**). The decrease of the metallic Co fraction is consistent with the reduction of m_s shown in **Figure 4d** and **Figure 5e**. Nevertheless, the XAS pattern acquired after positive voltage application shows greater presence of Co_3O_4 at the film's surface (blue curve, **Figure 6c**). This, together with the fact that m_s decreases even beyond its initial value (**Figure S4a**), suggests that an external source of oxygen coming from the PC could be plausible, since the amount of O within the film is limited. The origin of this excess of oxygen could be the inherent oxygen gas dissolved on the PC together with the OH^- ions formed during the electrolyte preparation (see **Experimental Section**)” This would support the increase of Co_3O_4 at the surface after applying +100 V. As noted, XAS detection depth is

limited to outermost nanometers from the surface, while VSM is an integrating technique, probing the whole film. This explains why the results gathered by both techniques seem to be contradictory, although they are not. Moreover, the increased amount of CoO and Co₃O₄ phases implies a more insulating surface, which further limits the XAS detection.

Regarding the Co–Pt/AlO_x film, the XAS spectrum of the untreated sample exhibits three main peaks (778.6, 779.2 and 779.9 eV) and a shoulder (777.6 eV) at the L₃ edge (black curve, **Figure S6a**), while a broad peak (794.4 eV) is observed at the L₂ edge (black curve, **Figure S6b**). The XAS pattern is consistent with a mixture of metallic Co, CoO and Co₃O₄, in agreement with the GIXRD results (**Figure 3**). No significant changes in the XAS spectrum are observed after subjecting the film to a negative voltage (blue curve, **Figure S6**). As mentioned earlier, the surface sensitivity of XAS technique is limited to the first nanometers from the surface while VSM-assisted magnetoelectric measurements involve the whole film volume. In this case, however, only small variations in the magnetic response were observed upon negative voltage application (**Figure 4b**), hence it is not surprising that no drastic changes are observed by XAS either. Moreover, according to previous works, magnetoelectric effects observed after applying negative voltage could arise from Al³⁺ diffusion into the Co–Pt film.⁵⁸ XAS provides information about Co in a metallic environment or in an oxide form. This means that Co in a metallic environment would be either Co–Co, Co–Pt, or Co–Al. Considering the fact that metallic Co and Co–Al would give almost indistinguishable spectra, this explains why the XAS spectrum remains unaltered after –100 V biasing. The Co–Pt/AlO_x film was not studied by XAS after positive voltage application because it was unstable (**Figure 5d,e and f**).

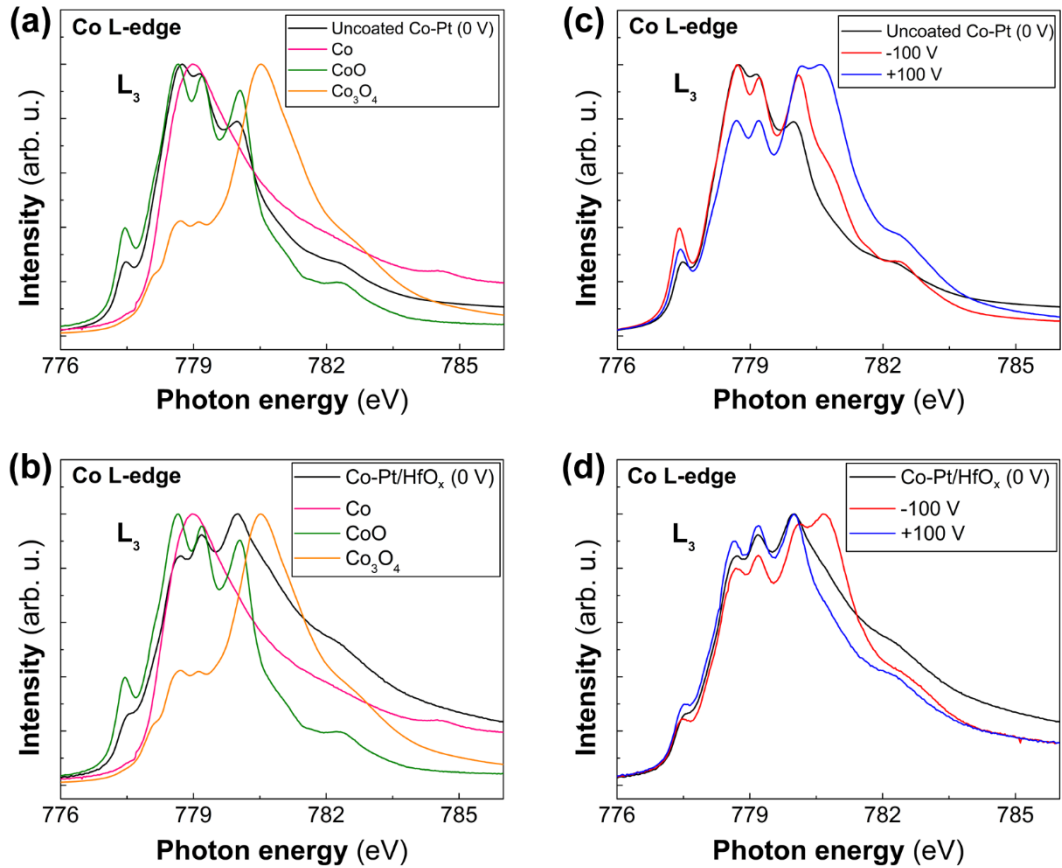


Figure 6. Zoom-in of the Cobalt L_3 -edge X-ray absorption spectra (XAS) of the as-prepared (0 V, black curve) (a) uncoated Co–Pt and (b) Co–Pt/ HfO_x films, together with the spectra of reference samples (pink: Co; green: CoO; orange: Co_3O_4). Evolution of the Cobalt L_3 -edge XAS after applying –100 V (red curve) and +100 V (blue curve) for (c) uncoated Co–Pt and (d) Co–Pt/ HfO_x films.

As for the Co–Pt/ HfO_x film is concerned, the XAS spectrum of the pristine sample at 0 V exhibits a multiplet structure consisting of four peaks (777.5, 778.7, 779.1 and 780 eV) at the L_3 edge and a peak (794.7 eV) at the L_2 edge (black curves, **Figure 6b** and **Figure S5b**). The multiplet is rather broad, especially the peak at 780 eV, which possesses higher intensity compared to the peaks at 777.5, 778.7 and 779.1 eV. This, together with the small intensity of the XMCD signal (black curve, **Figure 7**), indicates that the outermost surface of Co–Pt/ HfO_x film consists of a mixture of CoO, Co_3O_4 and some traces of metallic Co, in agreement with the GIXRD analysis (blue curve, **Figure 3**). When negative voltage is applied, the intensity of the shoulder (777.5 eV) and the two peaks at 778.7 and 779.1 eV on the L_3 edge slightly decrease, while the peak at 778 eV is shifted towards higher photon

energies (red curve, **Figure 6d**). The XAS spectrum also shows a new peak at 780.7 eV at the L₃ edge, while the main peak at the L₂ edge becomes sharpened. The latter matches the main peak of Co₃O₄ reference XAS (orange curve, **Figure 6b** and **Figure S5d**). Moreover, after subjecting the Co–Pt/HfO_x film to –100 V, the XMCD signal exhibits higher dichroism compared to the initial state (*i.e.* 0 V) (red curve, **Figure 7**). These results suggest the coexistence of Co₃O₄ and metallic Co at the surface of Co–Pt/HfO_x after applying negative voltage. When positive voltage is applied, the XAS spectrum exhibits a pattern similar to the initial state (0 V) at L₃ and L₂ edges (blue and black curves respectively, **Figure 6d** and **Figure S5d**), as well as a slight narrowing of the multiplet and a small intensity increase of the shoulder at 777.5 eV at the L₃ edge. Additionally, XMCD shows a decrease of the dichroic signal, almost recovering the initial state (blue curve, **Figure 7**). These results confirm that after applying positive voltage, the surface of Co–Pt/HfO_x films comprise CoO, metallic Co and some traces of Co₃O₄ in a proportion which differs only slightly from the pristine state (0 V). Note that the amount of surface oxides in the Co–Pt/HfO_x film after applying –100 V is clearly lower than for uncoated Co–Pt, thus corroborating the role of HfO_x as a good oxygen getter (poorer oxygen donor).⁴⁴ Since HfO_x is prone to accept oxygen (for negative voltages) rather than to donate it back to Co–Pt (for positive voltages), the magneto-ionic effects are more pronounced under negative biasing for Co–Pt/HfO_x.

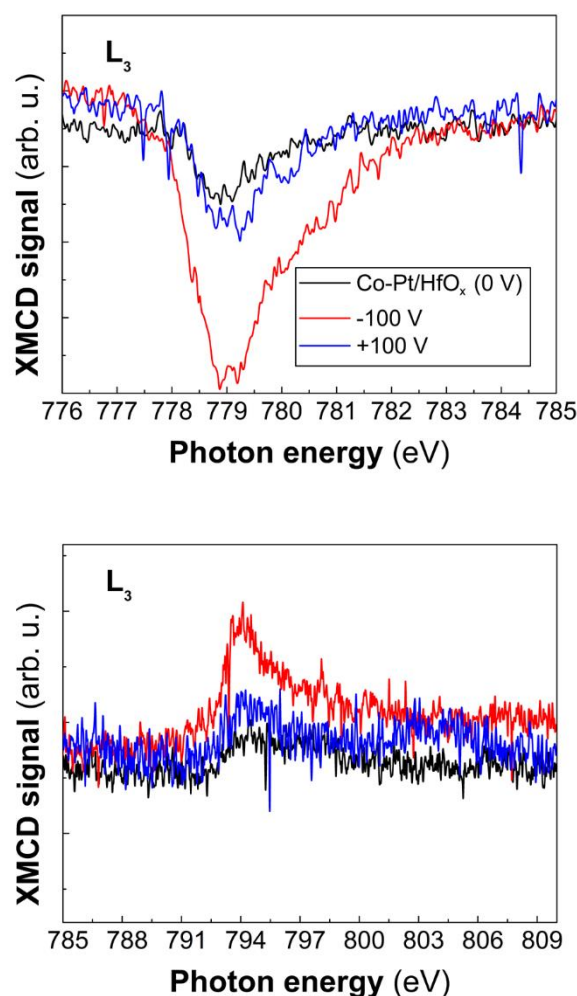


Figure 7. Zoom-in of the Cobalt L₃- and L₂-edge XMCD signal for the Co–Pt/HfO_x film in the pristine state (0V, black curve) and after applying –100 V (red curve) and +100 V (blue curve).

More specifically, as depicted in **Figure 8d,e**, the application of negative voltage to the Co–Pt/HfO_x system triggers the diffusion of O²⁻ ions from Co–Pt film towards the HfO_x layer, resulting in the partial reduction of Co₃O₄ to CoO and the reduction of CoO to metallic Co. Unlike the uncoated Co–Pt films, for which the O²⁻ migration was limited to the surface, oxygen ions can diffuse here within the HfO_x layer owing to the presence of oxygen vacancies in the HfO_x.^{60–63} Nevertheless, HfO_x is able to accept oxygen only to some extent. Oxygen anions not able to enter the HfO_x lattice are involved in the oxidation of a fraction of CoO to Co₃O₄ (**Figure 8e**). Thus, after applying negative voltages, the Co–Pt film shows a higher presence of metallic Co and some traces of Co₃O₄. This scenario is in accordance with the increase of m_S (**Figure 4c** and **Figure 5b**), the changes on the XAS

spectra (red curve, **Figure 6d**) and the increase of the dichroism in the XMCD signal (red curve, **Figure 7**). Conversely, when the electric field polarity is reversed, the sense of O^{2-} migration is inverted. Oxygen anions are partially released from the HfO_x towards the Co–Pt film, oxidizing part of the metallic Co to CoO and CoO to Co_3O_4 (**Figure 8f**). In this manner, the initial state (0 V) of the Co–Pt film tends to be recovered upon positive voltage application, although not entirely. This can be inferred from the decrease of m_S (**Figure S4c**), which does not reach the initial state (0 V), and the slight differences on the XAS spectra (black and blue curves, **Figure 6d**). The results indicate that amount of oxygen involved in the diffusion event under negative biasing does not completely diffuse back, even for large positive voltage. It is noteworthy that the observed changes in magnetism depending on the electric field polarity are in accordance with previous results reported for Co^{17,19,20} and with several studies devoted to O^{2-} migration in HfO_x under an electric field.^{64,65}

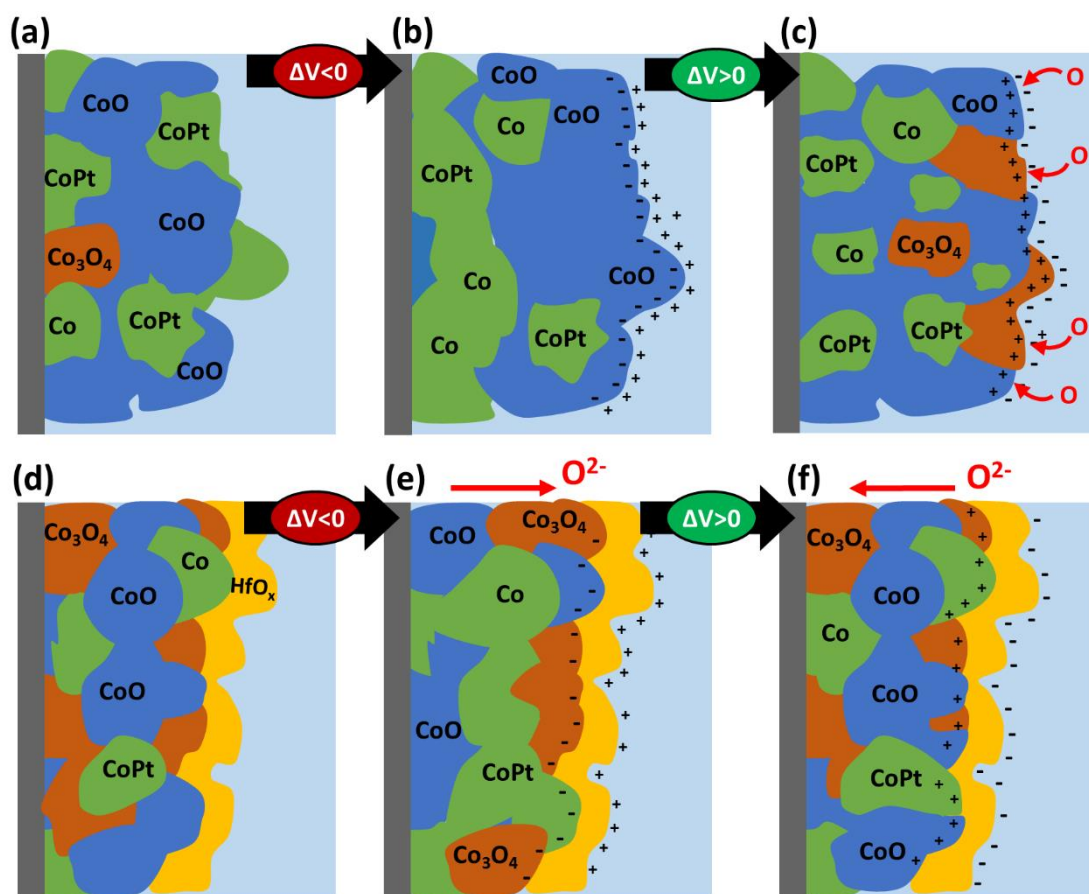


Figure 8. Schematic drawing of the distribution of cobalt phases in (a-c) uncoated Co–Pt and (d-f) Co–Pt/HfO_x films in (a,d) the pristine state (0 V), (b,e) when subject to $-\Delta V$ and (c,f) when subject to $+\Delta V$ in propylene carbonate (depicted as light blue medium).

The increase (and subsequent decrease) of H_C in the three systems investigated can also be related to the reduction of CoO to Co (and the subsequent oxidation to CoO), as reported in a previous study of ours on Co–Pt/CoO composite micro-disks.³¹ During negative voltage application, metallic Co regions might expand in size (**Figure 8b,e**). Considering that H_C is inversely proportional to the particle size within the multi-domain regime,⁶⁶ it is expected that H_C will decrease with the increase of Co(Pt) regions size. Conversely, the decrease of Co grain size (due to oxidation) (**Figure 8c,f**) would induce an increase of H_C . Dipolar interactions between de Co clusters must also be considered, since H_C can be reduced (enlarged) by enhancing (diminishing) the dipolar interactions.^{67,68} As the size of Co regions increases ($-\Delta V$), the distance between clusters is presumably reduced and Co(Pt)

clusters could even merge with each other (**Figure 8e**). Consequently, dipolar interactions would become stronger, leading to a decrease of H_C . The opposite would occur for positive voltages (**Figure 8c,e**). Finally, the opposite voltage-induced modulation trends for H_C and m_S could also be related to the relative influence of voltage on the effective magnetic anisotropy (K) and the saturation magnetization. Since H_C is proportional to K and inversely proportional to M_S (Stoner-Wolfarth model in the limiting case of non-interacting single domain particles), if M_S decreases faster than K for positive voltage polarity, this would cause an increase of H_C . In our case, this seems to be the case since, although we do not analyze K , there is marginal change in m_R/m_S (which is highly related to K) for the Co–Pt and Co–Pt/HfO_x systems at positive voltage. These effects have actually been reported in the literature.²⁰ Finally, if metallic Co produced from the reduction of CoO ($-\Delta V$) does not contain Pt (presumably opposite to the initial Co–Pt metallic regions in the as-deposited film), this is expected to also cause a reduction of H_C compared to the pristine hcp Co–Pt clusters.

CONCLUSIONS

In contrast to Co–Pt films, magneto-ionic effects in Co–Pt/AlO_x and Co–Pt/HfO_x heterostructures are enhanced due to the oxygen getter/donor capabilities of the adjacent oxide nanolayers. Large variations in H_C , m_S and m_R/m_S are obtained under negative and subsequent positive biasing. The electric field-driven migration of oxygen anions through the Co–Pt/oxide gate interface causes, in turn, variations in the Co oxidation state. These results demonstrate that coating nanostructured magnetic materials together with suitable insulating oxide nanolayers is an appealing strategy for boosting voltage-driven effects in magneto-ionic devices. In the future, we plan to operate the Co–Pt/AlO_x and Co–Pt/HfO_x in solid state by paying special attention to the occurrence of pinholes in the ALD layers. An investigation on the correlation between the thickness of the insulating layer and the probability of pinholes could be carried out in view of the optimum performance of the device.

Likewise, the concentration of oxygen vacancies in the non-stoichiometric HfO_x should be experimentally determined and its change correlated with the applied voltage.

ACKNOWLEDGEMENTS

Financial support by the European Research Council (SPIN-PORICS 2014-Consolidator Grant, Agreement n° 648454), the Spanish Government (Project MAT2017-86357-C3-1-R , MAT2017-83169-R “Severo Ochoa” Programme for Centres of Excellence in R&D SEV-2015-0496 and associated FEDER), the Generalitat de Catalunya (2017-SGR-292 and 2017-SGR-1519) and the European Union’s Horizon 2020 research and innovation programme under the Marie Skłodowska-Curie grant agreement n° 665919 is acknowledged. P.Y acknowledges Chinese Scholarship Council CSC fellowship (201606920073).

EXPERIMENTAL SECTION

Materials

HCl (Hydrochloric acid, 37 wt. %), isopropyl alcohol ($\text{C}_3\text{H}_8\text{O}$, 99.9%), acetone (99.0%), absolute ethanol (99.8%), $\text{Na}_2\text{PtCl}_6 \cdot 6\text{H}_2\text{O}$ (sodium hexachloroplatinate (IV) hexahydrate, 98.0%), CoCl_2 (cobalt(II) chloride anhydrous, $\geq 98.0\%$), and Pluronic P-123 ($\text{HO}(\text{CH}_2\text{CH}_2\text{O})_{20}(\text{CH}_2\text{CH}(\text{CH}_3)\text{O})_{70}(\text{CH}_2\text{CH}_2\text{O})_{20}\text{H}$) block copolymer, propylene carbonate (PC) (anhydrous, 99.7% purity, 0.002% or 20 ppm H_2O), trimethylaluminum, TMA [$(\text{CH}_3)_3\text{Al}$] and tetrakis(dimethylamido)hafnium, TDMAH [$((\text{CH}_3)_2\text{N})_4\text{Hf}$] were purchased from Sigma-Aldrich. Unless otherwise stated, the reagents were used as received without further purification. Deionized water was obtained through an EMD Millipore Simplicity™ Water Purification System (Millipore S.A.S., Molsheim 67120, France).

Samples fabrication

Nanostructured Co–Pt films were electrodeposited (ED) on Cu (70 nm)/Ti (10 nm)/Si substrates. ED was carried out in a three-electrode single-compartment cell connected to a PGSTAT302N Autolab potentiostat/galvanostat (Metrohm-Autolab). An Ag|AgCl double junction ($E = +0.210$ V SHE) with 3 M KCl inner solution and 1 M NaCl outer solution, was employed as reference electrode and a Pt spiral served as counter electrode. The films were deposited potentiostatically at -1.0 V during 600 s, under mild agitation ($\omega = 100$ rpm). The bath temperature was set at 25 °C. The electrolyte was prepared with Milli-Q water and contained 2.8 mM CoCl_2 , 1.3 mM $\text{Na}_2\text{PtCl}_6 \cdot 6\text{H}_2\text{O}$, and 1 $\text{mg} \cdot \text{mL}^{-1}$ (1 wt%) of Pluronic P-123. The pH was adjusted to 2.1 by adding 1 M HCl solution. The concentration of P-123 was chosen to be above its critical micellar concentration (c.m.c)⁶⁹ to induce the formation of P-123 micelles in the aqueous electrolyte. During the ED process, P-123 micelles get progressively in contact with the metal ions in solution and tend to get adsorbed on the cathode (working electrode) acting as a ‘structure directing agent’, and hence inducing the formation of tiny pores.^{14,31,42,43} No pH buffering agent was added to the bath so as not to preclude the incorporation of oxygen in the film, and therefore the resulting nanostructured films consisted of metallic Co–Pt and Co oxide phases. The thickness of the nanostructured Co–Pt films were measured to be around 150 nm.

AlO_x and HfO_x were deposited on the nanostructured Co–Pt films by atomic layer deposition (ALD) using a Cambridge NanoTech Savannah 100 reactor. AlO_x coatings were obtained by alternate pulsing of TMA and ozone in the reaction chamber in exposure mode, that is, by closing the gas exit valve for a certain amount of time to allow the precursors to diffuse into the pores and inter-grain channels of the Co–Pt films. Alternatively, HfO_x deposits were prepared by combining TDMAH (heated at 75 - 80 °C) and deionized water as co-reactant. High purity nitrogen gas was used as carrier and purging gas (40 and 20 sccm, respectively). In both cases, the chamber temperature was set at

200 °C. Film thickness was varied from 10 to 80 nm by modifying the number of the ALD cycles and was validated by X-ray reflectivity measurements on silicon (100) reference samples.

Morphology and structural characterization

Field emission scanning electron microscopy (FE-SEM) imaging and energy-dispersive X-ray (EDX) analyses were performed on a Zeiss MERLIN operated at 5 kV and 15 kV, respectively. Scanning transmission electron microscopy (STEM) images and electron energy loss spectroscopy (EELS) analyses were performed on a Tecnai F20 HRTEM/STEM microscope. The crystal structure was investigated by means of grazing incidence X-ray diffraction (GIXRD) using a Bruker-AXS, model A25 D8 Discover equipped with a LinxEye XE-T detector using Cu K α radiation and a grazing incidence angle of 1°.

X-ray absorption spectroscopy and X-ray magnetic circular dichroism characterization

The oxidation state of the nanostructured Co–Pt films were determined by X-ray absorption spectra (XAS) (Co L_{3,2} edges), measured in total electron yield (TEY) mode using linearly polarized light, at the UE46_PGM1 beamline (High-Field Diffractometer station of the synchrotron radiation source BESSY II, Helmholtz-Zentrum Berlin). To compare with reference XAS patterns, Co L_{3,2} edge XAS spectra of Co (20 nm-thick Co thin film, capped with 2 nm of Ta, grown by molecular beam epitaxy on top of a <100>-oriented MgO single crystal), CoO (Cobalt(II) oxide, 95%, powders from Alfa Aesar®) and sputtered Co₃O₄ film samples were also measured. X-ray magnetic circular dichroism (XMCD) was performed for further magnetic characterization, which records the difference in core-level absorption spectra (Co L_{3,2} edge) between right-handed (μ^+) and left-handed (μ^-) circularly polarized X-rays. XMCD measurements were carried out at room (300 K) under the applied magnetic fields of 20 and –20 kOe.

Magnetolectric measurements

Magnetic measurements were performed in a Micro Sense (LOT-Quantum Design) Vibrating Sample Magnetometer (VSM) at room temperature with a magnetic moment uncertainty of 0.5% and a coercivity uncertainty of ± 5 Oe. For *in situ* magneto-electric measurements, a homemade electrochemical cell was attached at the end of the VSM holder. The Co–Pt based films acted as the working electrode, a Pt wire as the counter electrode, and anhydrous propylene carbonate (PC) with a small amount of solvated Na^+ and OH^- species as the electrolyte (*i.e.* non-oxidative media). These were obtained upon treating the as-purchased PC with metallic sodium in order to remove any traces of residual water, thus minimizing corrosion events in the samples due to the electrolyte during magnetolectric measurements. Consequently, Na^+ and OH^- ions are formed which promote the formation electric double layer (EDL) and enhance the magnitude of the electric field in the samples.^{11,14,25,31,32} In-plane hysteresis loops were recorded applying different DC voltages ranging from 0 V to -100 V and 0 V to $+100$ V after waiting for 90 min at each voltage value, using an Agilent B2902A power supply as voltage source. Note that the voltage was maintained during the VSM measurements. Between the two series of voltage values, the electrolyte was restored to ensure optimized performance. Relative variation in H_C , m_S and m_R/m_S were determined as:

$$\Delta y (\%) = \frac{y_f - y_i}{y_i} \cdot 100$$

where y is the magnetic parameter under evaluation, y_i is its value at 0 V and y_f is the value at a given voltage. Note that y_i is different for the two series of voltage values ($0 \rightarrow -100$ V; $0 \rightarrow +100$).

ASSOCIATED CONTENT

Supporting Information.

The Supporting Information is available free of charge on the ACS Publications website at DOI:

This material includes SEM images, VSM measurements and XAS data.

REFERENCES

- (1) Chappert, C.; Fert, A.; Van Dau, F. N. The Emergence of Spin Electronics in Data Storage. *Nat. Mater.* **2007**, *6*, 813–823.
- (2) Dieny, B.; Sousa, R.; Herault, J.; Pappas, C.; Prenat, G.; Ebels, U.; Houssameddine, D.; Rodmacq, B.; Auffret, S.; Prejbeanu, L. B.; Cyrille, M.; Delaet, B.; Redon, O.; Ducruet, C.; Nozieres, J. P.; Prejbeanu, I. Spin-Transfer Effect and Its Use in Spintronic Components. *Int. J. Nanotechnol.* **2010**, *7*, 591–614.
- (3) Shiota, Y.; Nozaki, T.; Bonell, F.; Murakami, S.; Shinjo, T.; Suzuki, Y. Induction of Coherent Magnetization Switching in a Few Atomic Layers of FeCo Using Voltage Pulses. *Nat. Mater.* **2012**, *11*, 39–43.
- (4) Matsukura, F.; Tokura, Y.; Ohno, H. Control of Magnetism by Electric Fields. *Nat. Nanotechnol.* **2015**, *10*, 209–220.
- (5) Song, C.; Cui, B.; Li, F.; Zhou, X.; Pan, F. Recent Progress in Voltage Control of Magnetism: Materials, Mechanisms, and Performance. *Prog. Mater. Sci.* **2017**, *87*, 33–82.
- (6) Liu, M.; Obi, O.; Lou, J.; Chen, Y.; Cai, Z.; Stoute, S.; Espanol, M.; Lew, M.; Situ, X.; Ziemer, K. S.; Harris, V. G.; Sun, N. X. Giant Electric Field Tuning of Magnetic Properties in Multiferroic Ferrite/Ferroelectric Heterostructures. *Adv. Funct. Mater.* **2009**, *19*, 1826–1831.
- (7) Cherifi, R. O.; Ivanovskaya, V.; Phillips, L. C.; Zobelli, A.; Infante, I. C.; Jacquet, E.; Garcia, V.; Fusil, S.; Briddon, P. R.; Guiblin, N.; Mougín, A.; Ünal, A. A.; Kronast, F.; Valencia, S.; Dkhil,

- B.; Barthélémy, A.; Bibes, M. Electric-Field Control of Magnetic Order above Room Temperature. *Nat. Mater.* **2014**, *13*, 345–351.
- (8) Martin, L. W.; Ramesh, R. Multiferroic and Magnetoelectric Heterostructures. *Acta Mater.* **2012**, *60*, 2449–2470.
- (9) Bibes, M.; Barthélémy, A. Multiferroics: Towards a Magnetoelectric Memory. *Nat. Mater.* **2008**, *7*, 425–426.
- (10) Izyumskaya, N.; Alivov, Y.; Morkoç, H. Oxides, Oxides, and More Oxides: High-Oxides, Ferroelectrics, Ferromagnetics, and Multiferroics. *Crit. Rev. Solid State Mater. Sci.* **2009**, *34*, 89–179.
- (11) Dislaki, E.; Robbenolt, S.; Campoy-Quiles, M.; Nogués, J.; Pellicer, E.; Sort, J. Coercivity Modulation in Fe–Cu Pseudo-Ordered Porous Thin Films Controlled by an Applied Voltage: A Sustainable, Energy-Efficient Approach to Magnetoelectrically Driven Materials. *Adv. Sci.* **2018**, *5*, No. 1800499.
- (12) Weisheit, M.; Fähler, S.; Marty, A.; Souche, Y.; Poinignon, C.; Givord, D. Electric Field-Induced Modification of Magnetism in Thin-Film Ferromagnets. *Science*, **2007**, *315*, 349–351.
- (13) Ovchinnikov, I. V.; Wang, K. L. Theory of Electric-Field-Controlled Surface Ferromagnetic Transition in Metals. *Phys. Rev. B - Condens. Matter Mater. Phys.* **2009**, *79*, 1–4.
- (14) Quintana, A.; Zhang, J.; Isarain-Chávez, E.; Menéndez, E.; Cuadrado, R.; Robles, R.; Baró, M. D.; Guerrero, M.; Pané, S.; Nelson, B. J.; Müller, C. M.; Ordejón, P.; Nogués, J.; Pellicer, E.; Sort, J. Voltage-Induced Coercivity Reduction in Nanoporous Alloy Films: A Boost toward Energy-Efficient Magnetic Actuation. *Adv. Funct. Mater.* **2017**, *27*, 1–8.

- (15) Koyama, T.; Nakatani, Y.; Ieda, J. I.; Chiba, D. Electric Field Control of Magnetic Domain Wall Motion via Modulation of the Dzyaloshinskii-Moriya Interaction. *Sci. Adv* **2018**, *4*, eaav0265.
- (16) Bauer, U.; Yao, L.; Tan, A. J.; Agrawal, P.; Emori, S.; Tuller, H. L.; Van Dijken, S.; Beach, G. S. D. Magneto-Ionic Control of Interfacial Magnetism. *Nat. Mater.* **2015**, *14*, 174–181.
- (17) Bi, C.; Liu, Y.; Newhouse-Illige, T.; Xu, M.; Rosales, M.; Freeland, J. W.; Mryasov, O.; Zhang, S.; Te Velthuis, S. G. E.; Wang, W. G. Reversible Control of Co Magnetism by Voltage-Induced Oxidation. *Phys. Rev. Lett.* **2014**, *113*, 1–5.
- (18) Gilbert, D. A.; Olamit, J.; Dumas, R. K.; Kirby, B. J.; Grutter, A. J.; Maranville, B. B.; Arenholz, E.; Borchers, J. A.; Liu, K. Controllable Positive Exchange Bias via Redox-Driven Oxygen Migration. *Nat. Commun.* **2016**, *7*, 11050.
- (19) Zhou, X.; Yan, Y.; Jiang, M.; Cui, B.; Pan, F.; Song, C. Role of Oxygen Ion Migration in the Electrical Control of Magnetism in Pt/Co/Ni/HfO₂ Films. *J. Phys. Chem. C* **2016**, *120*, 1633–1639.
- (20) Yan, Y. N.; Zhou, X. J.; Li, F.; Cui, B.; Wang, Y. Y.; Wang, G. Y.; Pan, F.; Song, C. Electrical Control of Co/Ni Magnetism Adjacent to Gate Oxides with Low Oxygen Ion Mobility. *Appl. Phys. Lett.* **2015**, *107*, 122407.
- (21) Bauer, U.; Emori, S.; Beach, G. S. D. Voltage-Controlled Domain Wall Traps in Ferromagnetic Nanowires. *Nat. Nanotechnol.* **2013**, *8*, 411–416.
- (22) Dasgupta, S.; Das, B.; Knapp, M.; Brand, R. A.; Ehrenberg, H.; Kruk, R.; Hahn, H. Intercalation-Driven Reversible Control of Magnetism in Bulk Ferromagnets. *Adv. Mater.* **2014**, *26*, 4639–4644.

- (23) Leistner, K.; Lange, N.; Hänisch, J.; Oswald, S.; Scheiba, F.; Fähler, S.; Schlörb, H.; Schultz, L. Electrode Processes and in Situ Magnetic Measurements of FePt Films in a LiPF₆ based Electrolyte. *Electrochim. Acta* **2012**, *81*, 330–337.
- (24) Leistner, K.; Wunderwald, J.; Lange, N.; Oswald, S.; Richter, M.; Zhang, H.; Schultz, L.; Fähler, S. Electric-Field Control of Magnetism by Reversible Surface Reduction and Oxidation Reactions. *Phys. Rev. B - Condens. Matter Mater. Phys.* **2013**, *87*, 1–7.
- (25) Robbenolt, S.; Quintana, A.; Pellicer, E.; Sort, J. Large Magnetoelectric Effects Mediated by Electric-Field-Driven Nanoscale Phase Transformations in Sputtered (Nanoparticulate) and Electrochemically Dealloyed (Nanoporous) Fe-Cu Films. *Nanoscale* **2018**, *10*, 14570–14578.
- (26) Zhao, S.; Zhou, Z.; Peng, B.; Zhu, M.; Feng, M.; Yang, Q.; Yan, Y.; Ren, W.; Ye, Z. G.; Liu, Y.; Liu, M. Quantitative Determination on Ionic-Liquid-Gating Control of Interfacial Magnetism. *Adv. Mater.* **2017**, *29*, 1606478.
- (27) Diez, L. H.; Liu, Y.; Gilbert, D.; Belmeguenai, M.; Vogel, J.; Pizzini, S.; Martinez, E.; Lamperti, A.; Mohammedi, J.; Laborieux, A.; Roussigné, Y.; Grutter, A.; Arenholtz, E.; Quarterman, P.; Maranville, B.; Ono, S.; Hadri, M. S. E.; Tolley, R.; Fullerton, E.; Sanchez-Tejerina, L.; Stashkevich, A.; Chérif, S.; Kent, A.; Querlioz, D.; Langer, J.; Ocker, B.; Ravelosona, D. Nonvolatile Ionic Modification of the Dzyaloshinskii-Moriya Interaction. *Phys. Rev. Appl.* **2019**, *12*, 034005.
- (28) Gilbert, D. A.; Grutter, A. J.; Arenholz, E.; Liu, K.; Kirby, B. J.; Borchers, J. A.; Maranville, B. B. Structural and Magnetic Depth Profiles of Magneto-Ionic Heterostructures beyond the Interface Limit. *Nat. Commun.* **2016**, *7*, 1–8.
- (29) Jiang, M.; Chen, X. Z.; Zhou, X. J.; Cui, B.; Yan, Y. N.; Wu, H. Q.; Pan, F.; Song, C. Electrochemical Control of the Phase Transition of Ultrathin FeRh Films. *Appl. Phys. Lett.* **2016**, *108*, 202404

- (30) Hunter, R. J. *Foundations of Colloid Science*. Oxford University Press.: New York, 2001.
- (31) Navarro-Senent, C.; Fornell, J.; Isarain-Chávez, E.; Quintana, A.; Menéndez, E.; Foerster, M.; Aballe, L.; Weschke, E.; Nogués, J.; Pellicer, E.; Sort, J. Large Magnetoelectric Effects in Electrodeposited Nanoporous Microdisks Driven by Effective Surface Charging and Magneto-Ionics. *ACS Appl. Mater. Interfaces* **2018**, *10*, 44897–44905.
- (32) Quintana, A.; Menéndez, E.; Liedke, M. O.; Butterling, M.; Wagner, A.; Sireus, V.; Torruella, P.; Estradé, S.; Peiró, F.; Dendooven, J.; Detavernier, C.; Murray, P. D.; Gilbert, D. A.; Liu, K.; Pellicer, E.; Nogués, J.; Sort, J. Voltage-Controlled ON-OFF Ferromagnetism at Room Temperature in a Single Metal Oxide Film. *ACS Nano*. **2018**, *12*, 10291–10300.
- (33) Navarro-Senent, C.; Quintana, A.; Menéndez, E.; Pellicer, E.; Sort, J. Electrolyte-Gated Magnetoelectric Actuation: Phenomenology, Materials, Mechanisms, and Prospective Applications. *APL Mater.* **2019**, *7*, 030701.
- (34) Molinari, A.; Hahn, H.; Kruk, R. Voltage-Control of Magnetism in All-Solid-State and Solid/Liquid Magnetoelectric Composites. *Adv. Mater.* **2019**, 1806662.
- (35) Wagner, T.; Haffer, S.; Weinberger, C.; Klaus, D.; Tiemann, M. Mesoporous Materials as Gas Sensors. *Chem. Soc. Rev.* **2013**, *42*, 4036–4053.
- (36) Li, W.; Liu, J.; Zhao, D. Mesoporous Materials for Energy Conversion and Storage Devices. *Nature Reviews Materials*. **2016**, *1*, 16023.
- (37) Pal, N.; Bhaumik, A. Mesoporous Materials: Versatile Supports in Heterogeneous Catalysis for Liquid Phase Catalytic Transformations. *RSC Advances*, **2015**, *5*, 24363–24391.

- (38) Reitz, C.; Suchomski, C.; Wang, D.; Hahn, H.; Brezesinski, T. In Situ Tuning of Magnetization via Topotactic Lithium Insertion in Ordered Mesoporous Lithium Ferrite Thin Films. *J. Mater. Chem. C* **2016**, *4*, 8889–8896.
- (39) Ghosh, S. Charge-Response of Magnetization in Nanoporous PdNi Alloys. *J. Magn. Magn. Mater.* **2011**, *32*, 552–556.
- (40) Quintana, A.; Menéndez, E.; Isarain-Chávez, E.; Fornell, J.; Solsona, P.; Fauth, F.; Baró, M. D.; Nogués, J.; Pellicer, E.; Sort, J. Tunable Magnetism in Nanoporous CuNi Alloys by Reversible Voltage-Driven Element-Selective Redox Processes. *Small* **2018**, *14*, 1704396.
- (41) Dubraja, L. A.; Reitz, C.; Velasco, L.; Witte, R.; Kruk, R.; Hahn, H.; Brezesinski, T. Electrochemical Tuning of Magnetism in Ordered Mesoporous Transition-Metal Ferrite Films for Micromagnetic Actuation. *ACS Appl. Nano Mater.* **2017**, *1*, 65.
- (42) Isarain-Chávez, E.; Baró, M. D.; Alcantara, C.; Pané, S.; Sort, J.; Pellicer, E. Micelle-Assisted Electrodeposition of Mesoporous Fe–Pt Smooth Thin Films and Their Electrocatalytic Activity towards the Hydrogen Evolution Reaction. *ChemSusChem* **2018**, *11*, 367–375.
- (43) Zhang, J.; Quintana, A.; Menéndez, E.; Coll, M.; Pellicer, E.; Sort, J. Electrodeposited Ni-Based Magnetic Mesoporous Films as Smart Surfaces for Atomic Layer Deposition: An “All-Chemical” Deposition Approach toward 3D Nanoengineered Composite Layers. *ACS Appl. Mater. Interfaces* **2018**, *10*, 14877.
- (44) Foster, A. S.; Shluger, A. L.; Nieminen, R. M. Mechanism of Interstitial Oxygen Diffusion in Hafnia. *Phys. Rev. Lett.* **2002**, *89*, 1–4.
- (45) Aschauer, U.; Bowen, P.; Parker, S. C. Oxygen Vacancy Diffusion in Alumina: New Atomistic Simulation Methods Applied to an Old Problem. *Acta Mater.* **2009**, *57*, 4765–4772.

- (46) Wang, D.; He, G.; Hao, L.; Gao, J.; Zhang, M. Comparative Passivation Effect of ALD-Driven HfO₂ and Al₂O₃ Buffer Layers on the Interface Chemistry and Electrical Characteristics of Dy-Based Gate Dielectrics. *J. Mater. Chem. C* **2019**, *7*, 1955–1965.
- (47) Wang, L. G.; Qian, X.; Cao, Y. Q.; Cao, Z. Y.; Fang, G. Y.; Li, A. D.; Wu, D. Excellent Resistive Switching Properties of Atomic Layer-Deposited Al₂O₃/HfO₂/Al₂O₃ Trilayer Structures for Non-Volatile Memory Applications. *Nanoscale Res. Lett.* **2015**, *10*, 135.
- (48) Wang, C.; Zhang, H.; Li, C.; He, Y.; Zhang, L.; Zhao, X.; Yang, Q.; Xian, D.; Mao, Q.; Peng, B.; Zhou, Z.; Cui, W.; Hu, Z. Voltage Control of Magnetic Anisotropy through Ionic Gel Gating for Flexible Spintronics. *ACS Appl. Mater. Interfaces* **2018**, *10*, 29750
- (49) Zhao, S.; Zhou, Z.; Li, C.; Peng, B.; Hu, Z.; Liu, M. Low-Voltage Control of (Co/Pt)_x Perpendicular Magnetic Anisotropy Heterostructure for Flexible Spintronics. *ACS Nano* **2018**, *12*, 7167–7173.
- (50) Yang, Q.; Zhou, Z.; Wang, L.; Zhang, H.; Cheng, Y.; Hu, Z.; Peng, B.; Liu, M. Ionic Gel Modulation of RKKY Interactions in Synthetic Anti-Ferromagnetic Nanostructures for Low Power Wearable Spintronic Devices. *Adv. Mater.* **2018**, *30*, 1800449.
- (51) Jiang, Y.; Liu, N.; Gerung, H.; Cecchi, J.; Brinker, C. Nanometer-Thick Conformal Pore Sealing Of Self-Assembled Mesoporous Silica By Plasma-Assisted Atomic Layer Deposition. *J. Am. Chem. Soc.* **2006**, *128*, 11018-11019.
- (52) Darling, A. S.; Mech. E., A. M. Cobalt–Platinum Alloys A Critical Review of Their Constitution and Properties. *Platin. Met. Rev.* **1963**, *7*, 96–104.
- (53) Miller, M. S.; Schultz, A. E.; Chow, Y. M.; Heuer, L. A. Optimization of Co–Pt and Co–Cr–Pt–Ta Thin Films for Use in Magnetic Data Storage Devices. *Surf. Coatings Technol.* **1994**, *68/69*, 696–701.

- (54) Lin, T. Magnetic, Recording and Structural Characteristics of Sputtered Co–Cr–Pt Films for Longitudinal Recording. *J. Magn. Magn. Mater.* **1990**, *86*, 159.
- (55) Cui, B.; Song, C.; Gehring, G. A.; Li, F.; Wang, G.; Chen, C.; Peng, J.; Mao, H.; Zeng, F.; Pan, F. Electrical Manipulation of Orbital Occupancy and Magnetic Anisotropy in Manganites. *Adv. Funct. Mater.* **2015**, *25*, 864–870.
- (56) Liu, Y. T.; Ono, S.; Agnus, G.; Adam, J. P.; Jaiswal, S.; Langer, J.; Ocker, B.; Ravelosona, D.; Herrera Diez, L. Electric Field Controlled Domain Wall Dynamics and Magnetic Easy Axis Switching in Liquid Gated CoFeB/MgO Films. *J. Appl. Phys.* **2017**, *122*, 133907.
- (57) Sahadevan, A. M.; Kalitsov, A.; Kalon, G.; Bhatia, C. S.; Velez, J.; Yang, H. Electric-Field-Induced Magnetization Changes in Co/Al₂O₃ Granular Multilayers. *Phys. Rev. B - Condens. Matter Mater. Phys.* **2013**, *87*, 014425.
- (58) Cheng, B.; Qin, H.; Liu, L.; Xie, J.; Zhou, G.; Chen, L.; Hu, J. Electric-Field Control of Magnetic Properties for α -Fe₂O₃/Al₂O₃ Films. *J. Phys. D. Appl. Phys.* **2018**, *51*, 235002.
- (59) Miwa, S.; Suzuki, M.; Tsujikawa, M.; Matsuda, K.; Nozaki, T.; Tanaka, K.; Tsukahara, T.; Nawaoka, K.; Goto, M.; Kotani, Y.; Ohkubo, T.; Bonell, F.; Tamura, E.; Hono, K.; Nakamura, T.; Shirai, M.; Yuasa, S.; Suzuki, Y. Voltage Controlled Interfacial Magnetism through Platinum Orbits. *Nat. Commun.* **2017**, *8*, 15848.
- (60) Chen, T. J.; Kuo, C. L. Oxygen Vacancy Formation and the Induced Defect States in HfO₂ and Hf-Silicates - A First Principles Hybrid Functional Study. *Microelectron. Reliab.* **2014**, *54*, 1119-1124.
- (61) Xu, D. P.; Yu, L. J.; Chen, X. D.; Chen, L.; Sun, Q. Q.; Zhu, H.; Lu, H. L.; Zhou, P.; Ding, S. J.; Zhang, D. W. In Situ Analysis of Oxygen Vacancies and Band Alignment in HfO₂/TiN Structure for CMOS Applications. *Nanoscale Res. Lett.* **2017**, *12*, 311.

- (62) Tse, K.; Liu, D.; Xiong, K.; Robertson, J. Oxygen Vacancies in High-k Oxides. *Microelectron. Eng.* **2007**, *84*, 2028–2031.
- (63) Perevalov, T. V.; Aliev, V. S.; Gritsenko, V. A.; Saraev, A. A.; Kaichev, V. V. Electronic Structure of Oxygen Vacancies in Hafnium Oxide. *Microelectron. Eng.* **2013**, *109*, 21–23.
- (64) Goux, L.; Czarnecki, P.; Chen, Y. Y.; Pantisano, L.; Wang, X. P.; Degraeve, R.; Govoreanu, B.; Jurczak, M.; Wouters, D. J.; Altimime, L. Evidences of Oxygen-Mediated Resistive-Switching Mechanism in TiN/HfO₂/Pt Cells. *Appl. Phys. Lett.* **2010**, *97*, 243509.
- (65) Nagata, T.; Haemori, M.; Yamashita, Y.; Yoshikawa, H.; Iwashita, Y.; Kobayashi, K.; Chikyow, T. Oxygen Migration at Pt/HfO₂/Pt Interface under Bias Operation. *Appl. Phys. Lett.* **2010**, *97*, 082902.
- (66) Hadjipanayis, G. C. Nanophase Hard Magnets. *J. Magn. Magn. Mater.* **1999**, *200*, 373–391.
- (67) Kechrakos, D.; Trohidou, K. Magnetic Properties of Dipolar Interacting Single-Domain Particles. *Phys. Rev. B - Condens. Matter Mater. Phys.* **1998**, *58*, 12169–12177.
- (68) Skomski, R.; Coey, J. M. D. *Permanent Magnetism*; Institute of Physics Publishing: Bristol, 1999.
- (69) Wanka, G.; Hoffmann, H.; Ulbricht, W. Phase Diagrams and Aggregation Behavior of Poly(Oxyethylene)-Poly(Oxypropylene)-Poly(Oxyethylene) Triblock Copolymers in Aqueous Solutions. *Macromolecules* **1994**, *27*, 4145–4159.

Table of Contents (TOC) figure

